

# **Arctic sea ice extent and melt onset from NSCAT observations**

Simon H. Yueh and R. Kwok

Jet Propulsion Laboratory, California Institute of Technology, Pasadena, California

Short title: NSCAT OBSERVATIONS OF ARCTIC SEA ICE

**Abstract.** Arctic sea ice extent and the timing of melt onset are important parameters in the study of polar processes and climate changes. NSCAT Ku-band active microwave observations of the Arctic sea ice cover are described in this article with emphasis on their potential use for estimating ice extent and detection of spring melt. The NSCAT Arctic sea ice extent was found to have a reasonable agreement with the SSM/I winter ice extent. For spring melt-onset, a comparative study of NSCAT sea ice observations and surface air temperature indicates that Ku-band backscatter of the snow cover over multi-year ice has a clear and steep change as the surface temperature rises above freezing, similar to what was observed in previous investigations using ERS-1 C-band SAR observations. This signature of melt onset should provide a useful large-scale estimate of the dates of melt onset. A more extensive validation of the potential of this dataset is definitely suggested.

## 1. Introduction

In this paper, we illustrate the potential of using spaceborne Ku-band scatterometer observations for estimation of the areal extent of the sea ice cover and the detection of melt onset in the spring. The NASA Scatterometer (NSCAT) [*Naderi et al.*, 1992], launched on the Japanese Advanced Earth Observation Satellite (ADEOS) in August 1996, is a Ku-band (13.995 GHz) microwave radar, designed to measure global ocean wind fields. Although the NSCAT mission was terminated at the end of June 1997 due to the failure of ADEOS solar panel, it has acquired a large enough dataset to enable a closer examination of active Ku-band radar signatures of Arctic sea ice from fall to early summer.

The seasonal cycle of growth and decay of the ice cover is dependent on insolation and the variability of atmospheric and oceanic forcings on interannual and decadal time scales. The time series of ice extent derived from recent satellite passive microwave record (1978-1996) show an almost 3%/decade decrease and a 1.3%/decade increase in the area of the ice cover in the Arctic and Antarctic since 1978 [*Cavalieri et al.*, 1997]. NSCAT is the first active microwave sensor, with comparable spatial and temporal coverage, to provide a complementary view of the entire sea ice cover and may serve to improve our understanding of the estimates of areal extents from satellite passive microwave data.

The length of the melt season over the sea ice cover is defined by two transitions: melt onset and freeze-up. A large decrease in surface albedo accompanies the onset of snow melt during the spring and thus increases the absorption and heating of the ice by shortwave radiation. The rapid temperature decrease during freeze-up in the fall has an opposite effect on albedo and marks the beginning of the ice growth season and the end of the summer. These transitions have profound effects on the surface energy balance. The advance and retreat of the 0 deg C isotherm and the length of the melt season are parameters that may serve as sensitive indicators of climate change in the high

latitudes. Winebrenner et al. (1994) and Winebrenner et al. (1996) have demonstrated that the onset of melt and freeze-up events are clearly detectable as changes in radar backscatter in C-band ERS-1 Synthetic Aperture Radar (SAR) imagery. During melt onset, the appearance of liquid water in the snow cover on multiyear ice is marked by a steep decrease (almost 9 dB) in the observed backscatter. We demonstrate here the sensitivity of the NSCAT observations at 14 Ghz to be similar to that of 5 Ghz ERS SAR data. However, a frequent and wide swath coverage provided by NSCAT enables large scale observations of these seasonal transitions, complementing available passive microwave radiometer and high resolution SAR measurements [Anderson, 1997; Smith, 1998; Comiso and Kwok, 1996].

## 2. NSCAT Data: September 96-June 1997

NSCAT operates six fan beam antennas illuminating two single-sided 600 km swaths [Naderi et al., 1992]. The fore- and aft- antennas operate at vertical polarization, while the mid-beam antennas acquire vertically and horizontally polarized backscatter. The ratio of the vertically and horizontally polarized returns (polarization ratio) at incidence angles above 40 degrees has been found to be an effective discriminator between sea ice and open water samples [Yueh et al., 1997]. A simple algorithm for ice/water classification was developed using the polarization ratio and backscatter intensities (interpolated to 50 degree incidence angle) [Yueh et al., 1997]. We apply this ice/water classifier to NSCAT data sampled to a 25 km Special Sensor Microwave/Image (SSM/I) grid based on the locations of cell centers. The polarization ratios are averages of observations above 40 degree incidence acquired by the middle beam from multiple satellite passes. We also use the near-simultaneous NSCAT data from all antenna beams and all incidence angles to estimate the backscatter on a 12.5 km SSM/I grid using the

following linear backscatter model [Yueh *et al.*, 1997]:

$$\sigma_0(dB) = A + B(\theta - 50) \quad (1)$$

where  $\theta$  is the incidence angle in degrees. The coefficients  $A$  and  $B$  are estimated using the least-squares criterion with the squared-difference between every NSCAT measurement and the linear model weighted by the areal fraction of the  $\sigma_0$  cell falling inside the 12.5 km x 12.5 km SSM/I bins. The average polarization ratios and the estimates of  $A$  are subsequently used to classify sea ice and water on the 25 km SSM/I grids. Because this algorithm uses only NSCAT mid-beam polarization ratios above 40 degree incidence, it requires about 3 days of data to complete the classification of the entire Arctic region because of reduced spatial coverage.

Figure 1 illustrates the Ku-band backscatter images ( $A$  in dB) of Arctic sea ice from September 1996 to June 1997. From fall through early spring, multi-year (MY) sea ice is frozen with a snow cover. The scattering from the MY ice volume, snow grains, hummocky ice surfaces and ridges within an NSCAT resolution cell results in a remarkably uniform backscatter level typically above -12 dB (yellow to orange colors in Figure 1). The higher salinity first year (FY) ice cover has a smoother surface and thus has a low backscatter (typically less than -14 dB). The contrast between MY and FY ice backscatter levels is quite significant in comparison with the 0.3 dB estimated calibration accuracy of the scatterometer data. The areal coverage of FY sea ice is small at the end of melt-season but increases rapidly after fall freeze-up. From September to March, it appears that the area of perennial MY ice cover (orange color) near the central Arctic has reduced, likely due to the advection of sea ice primarily through the Fram strait to the Greenland sea. Near the middle of May, the rapid retreat of the ice is evident as rising surface air temperature melts the thinner first-year ice. A significant drop in MY ice backscatter, as melt water starts to appear in the snow layer, occurred around the second week of June and coincided well with the time of melt onset.

An interesting sea ice feature, the Odden ice tongue in the Greenland Sea, was noticeable from mid-November through early April. The Odden ice tongue, which failed to develop during both 1994 and 1995, was associated with mid-gyre convection and has been suggested as an indicator of climate changes. Since the Odden ice tongue consists largely of frazil and pancake ice, a successful detection of Odden ice tongue lends support to the applicability of polarization ratio for discriminating open water and young sea ice.

### **3. Comparison with SSM/I Ice Extent**

Here, we compare the NSCAT and SSM/I ice extents in a square domain within the  $\pm 3000$  km SSM/I grids centered at pole. Figure 2 illustrates the NSCAT and SSM/I ice extents for the entire period of NSCAT operation. The SSM/I ice extents were averaged over the same period of time required to create an NSCAT composite - 3 days. (We find that daily SSM/I images are noisy and occasionally had a significant data gap in this box. Therefore we use a threshold of  $1.0 \times 10^6$  square km to discard any daily ice concentration images with a large data gap from our analysis.) The SSM/I ice extents were calculated with two different thresholds: 15 and 25 percent ice concentration. Pixels with ice concentration above these thresholds are included in the ice extent calculation - SSM/I ice extents are typically computed using the 15 percent threshold. In general, NSCAT ice extent agrees reasonably well with the SSM/I ice extent defined by 25 percent concentration in winter. In particular, both data sets have detected consistent fluctuations of ice extent from February 10 through the end of April 1997. The results shown here suggest that NSCAT ice extent using a polarization ratio threshold of 2 dB corresponds to approximately the SSM/I ice extent computed using the 25 percent ice concentration threshold. However, if the threshold of backscatter polarization ratio is increased for ice and water discrimination, the number of pixels classified into ice will increase and the results will approach that defined by 15 percent

ice concentration. The thresholds in NSCAT and SSM/I ice/water detection algorithms are selected based on our tolerance to error and noise. We believe that since NSCAT data are relatively insensitive to atmospheric effects, these measurements will serve to enhance our understanding of ice extent.

#### 4. Melt Onset

Fig. 3 shows the spatial distribution of backscatter of the Arctic Ocean sea ice cover between May 29 and June 18. The temperature contours with the 0 deg C isotherm (in bold red), overlaid on the backscatter map is derived from NCEP reanalyzed temperature fields. The large region of high backscatter (yellow to orange) north of Greenland and the high Arctic is probably an area of older, less saline and deformed ice. The motion of the 0 deg C isotherm shows the advance of the warming trend into the Arctic Ocean. The onset of melt propagated from the Bering Strait towards the north pole and northern Greenland. As liquid water appears over the snow cover on multiyear ice, we observe a steep decrease in the backscatter. By mid-June, the high backscatter regions have all but disappeared from the ice cover. In the last backscatter map of the sequence, the only areas of high backscatter left are those north of Greenland. During this short period of three weeks, most of the Arctic has experienced a melt event which is unmistakable in the backscatter data from NSCAT.

We also correlated the backscatter and temperature time series at four points around the Arctic (Fig. 4) - the location of these points are indicated in the upper left panel in Fig. 3 by A, B, C, and D. There is quite a remarkable correspondence between a sharp drop in the backscatter and the zero crossing of the temperature record at those points. It appears that if -12 dB threshold is selected for estimating the date of melt onset, the NSCAT estimate will agree with NCEP/NCAR reanalysis to within +/- 2 days at these locations. It should be noted that since our NSCAT backscatter images are 3-day composites, the timing uncertainty of melt onset indicated in these NSCAT

images is  $\pm 1.5$  days. Investigations using data from a less number of satellite passes for melt onset detection to improve the resolution of temporal sampling are desirable.

## 5. Summary

The potential use of NSCAT data for monitoring the sea ice extent and onset of melt onset were illustrated. The NSCAT observations appear to support the validity of winter sea ice extent derived from SSM/I. In the winter, our NSCAT ice extent estimates, using a polarization threshold of 2 dB, compares well with the SSM/I ice extent estimates using a 25 percent sea ice concentration threshold. However, there are non-negligible differences during early summer and fall which might be due to differing sensitivities of active and passive microwave observations to atmosphere effects and the thermal conditions of the ice surface particularly at the ice edge. The signature of Ku-band backscatter of the MY sea ice cover is highly sensitive to melt onset. We observe a steep decrease of about 9 to 12 dB backscatter over the MY ice cover when free water starts appearing in the snow layer in the spring. The qualitative comparison with NCAR/NCEP temperature reanalysis seems reasonable. Nevertheless, there are some apparent discrepancies between the dates of significant NSCAT  $\sigma_0$  changes and the time when the NCEP/NCAR reanalysis reaches 0 degree C. Our first analysis shows that estimates of the date of melt onset on MY ice can be made with spaceborne Ku-band radar observations. We believe that this is a valuable dataset for monitoring the polar regions and more extensive validation studies of the parameters investigated here are warranted.

**Acknowledgments.** G. Cunningham of JPL provided valuable assistance in the processing and analysis of SSM/I ice concentration grids and NCEP/NCAR reanalysis. We are grateful to National Snow and Ice Data Center for making the daily SSM/I ice concentration grids available for this investigation. We also thank the NCAR/NCEP Reanalysis data

provided through the NOAA Climate Diagnostics Center (<http://www.cdc.noaa.gov/>).

This work was performed under contract with the National Aeronautics and Space Administration at the Jet Propulsion Laboratory, California Institute of Technology.

## References

- Anderson, M. R., Determination of a melt-onset date for Arctic sea-ice regions using passive-microwave data, *Annals of Glaciology*, 25, 382, 1997.
- Cavalieri, D. J., P. Gloersen, C. I. Parkinson, J. C. Comiso, and H. Zwally, Observed hemispheric-asymmetry in global sea ice changes, *Science*, Vol. 278, 1104-1106, Nov. 1997.
- Comiso, J. C. and R. Kwok, Surface and radiative characteristics of the summer Arctic sea ice cover from multisensor satellite observations, *J. Geophys. Res.*, 101(C12), 28397-28416, 1996.
- Naderi, F. M., M. H. Freilich, and D. G. Long, Spaceborne Radar Measurement of Wind Velocity Over the Ocean — An Overview of the NSCAT Scatterometer System, *Proc. of The IEEE*, Vol. 79, No. 6, 850-866, 1991.
- Smith, D. M., Recent increase in the length of the melt season of perennial Arctic sea ice, *Geophys. Res. Lett.*, 655-658, 1998.
- Winebrenner, D. P., E. D. Nelson, R. Colony, and R. D. West, Observations of melt onset on multiyear Arctic sea ice using the ERS 1 synthetic aperture radar, *J. Geophys. Res.*, 99(C11), 22425-22441, 1994.
- Winebrenner, D. P., B. Holt, and E. D. Nelson, Observation of autumn freeze-up in the Beaufort and Chukchi Seas using the ERS-1 synthetic aperture radar, *J. Geophys. Res.*, 101(C7), 16401-16419, 1996.
- Yueh, S. H., R. Kwok, S.-H. Lou, and W.-Y. Tsai, Sea ice identification using dual-polarized Ku-band scatterometer data, *IEEE Trans. Geosci. Remote Sens.*, Vol. 35, No. 3, 560-569, 1997.

---

S. H. Yueh and R. Kwok, Jet Propulsion Laboratory, California Institute of Technology, 4800 Oak Grove Drive, Pasadena, CA 91109. (e-mail: [simon@stokes2.jpl.nasa.gov](mailto:simon@stokes2.jpl.nasa.gov); [ron@rgps.jpl.nasa.gov](mailto:ron@rgps.jpl.nasa.gov))

Received \_\_\_\_\_

**Figure 1.** Ku-band microwave signatures of Arctic sea ice from fall 1996 through June 1997. The period of NSCAT data processed for each image is indicated on the top of each image with the first two digits for year, the next two digits for month and the last two digits for day.

**Figure 2.** Comparison of NSCAT and SSM/I Arctic sea ice extents within the  $\pm 3000$  km square box (SSM/I grids) centered at pole. The upper panel compares average SSM/I ice extent and NSCAT ice extent, while the lower panel illustrates daily SSM/I ice extent. (SSM/I ice concentration images with a coverage gap larger than  $1.0 \times 10^6$  square km have been excluded for illustration.)

**Figure 3.** NSCAT sea ice backscatter and NCEP surface temperature reanalysis during melt-onset.

**Figure 4.** Temporal evolutions of MY sea ice backscatter during melt-onset.

# NSCAT SEA ICE SIGMA0

Ice Edge Defined by Polarization Ratio and Backscatter

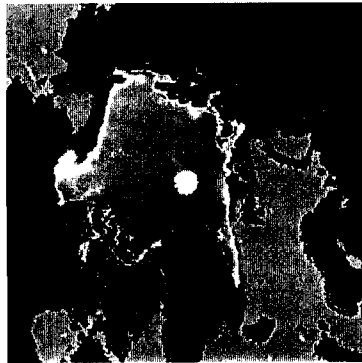
960919-960923



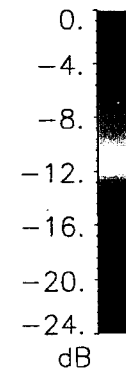
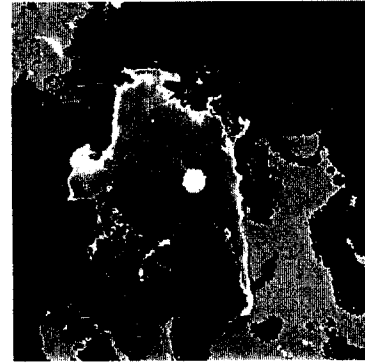
961016-961020



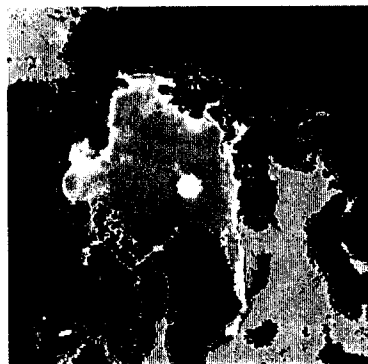
961109-961113



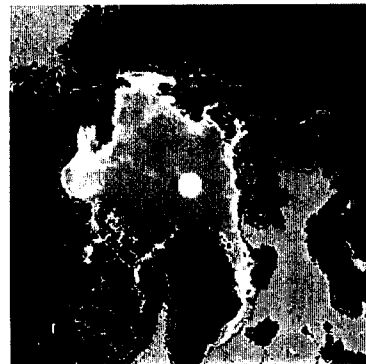
961130-961204



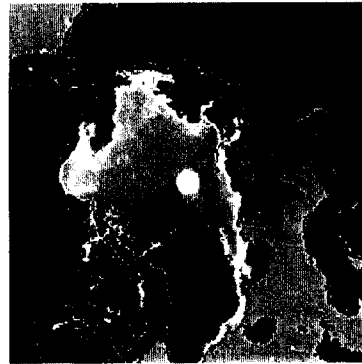
961215-961218



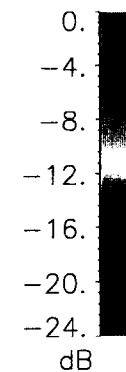
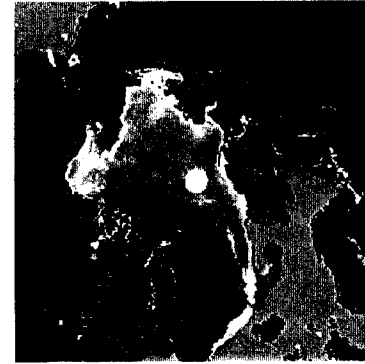
970117-970120



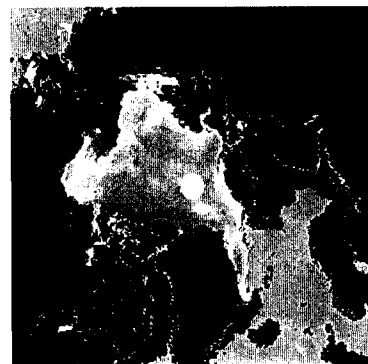
970215-970219



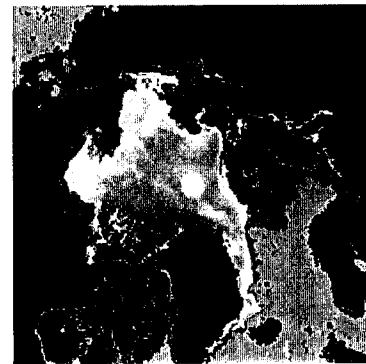
970315-970319



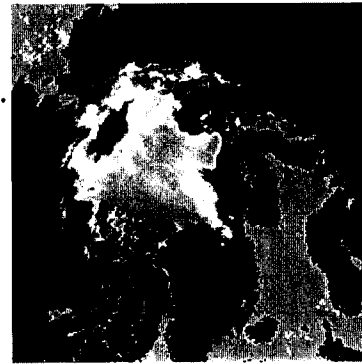
970412-970416



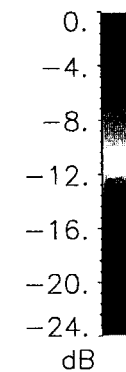
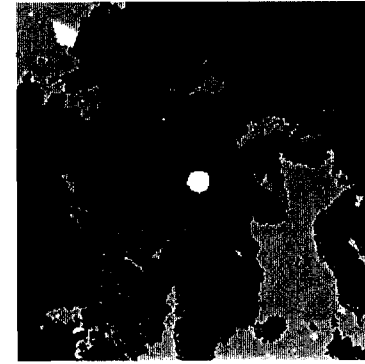
970430-970503



970531-970604

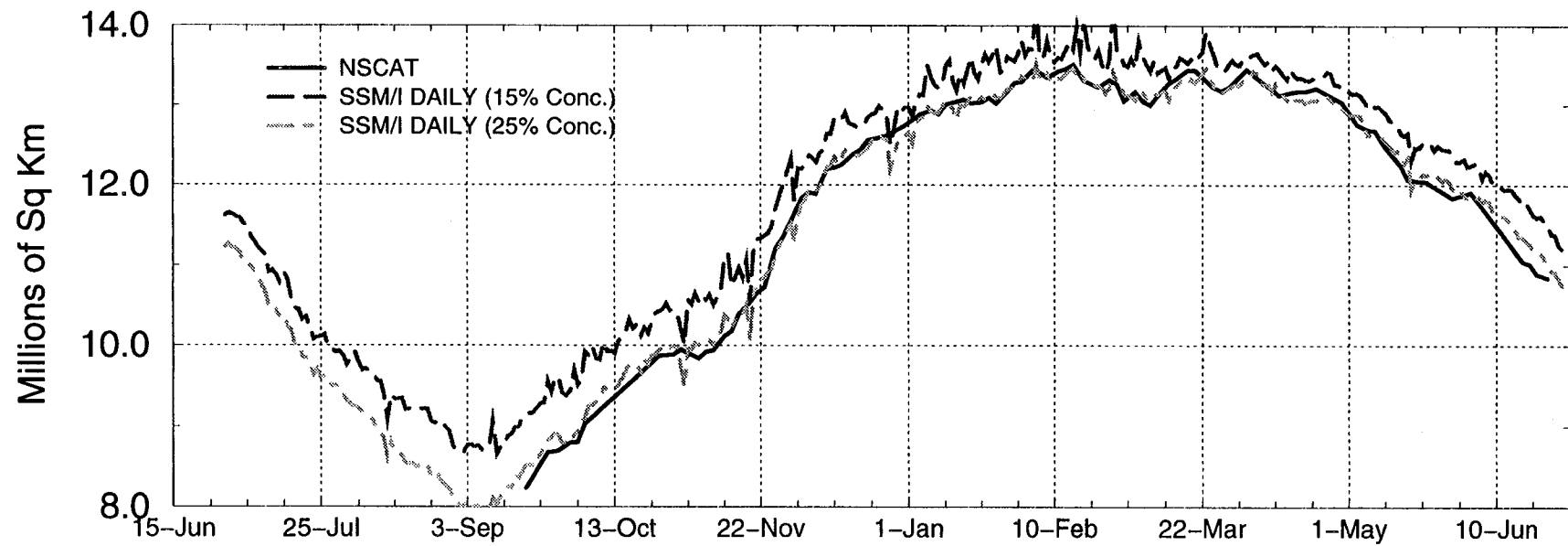
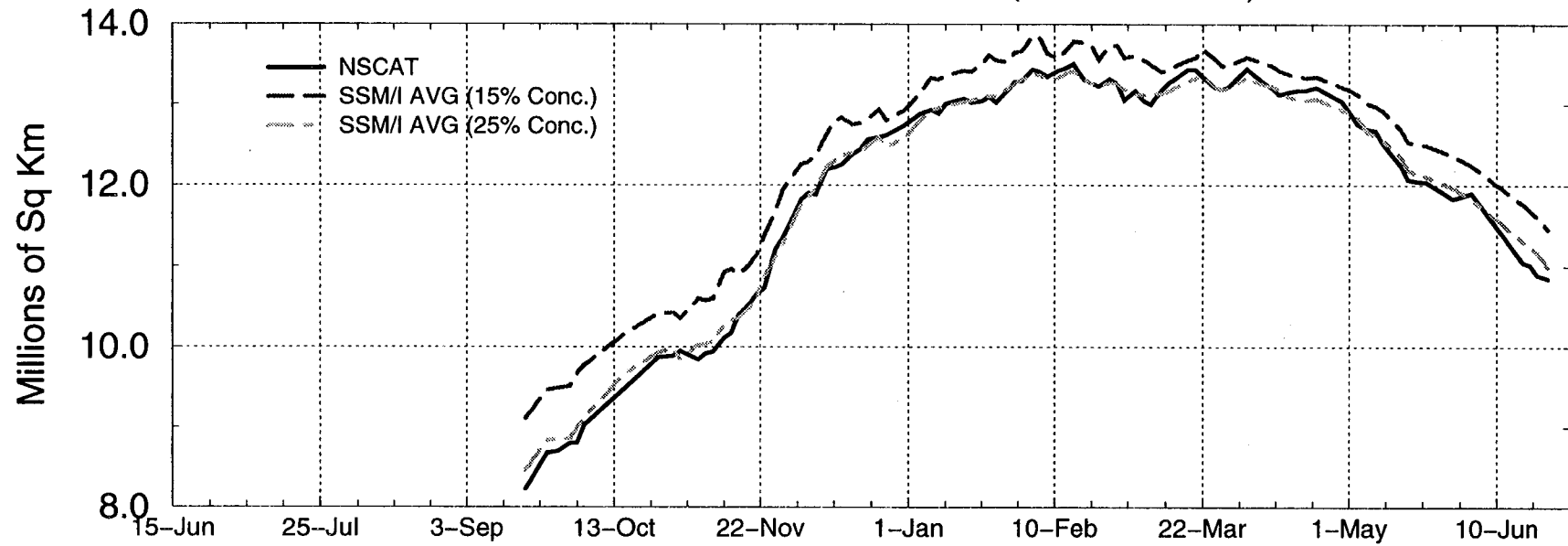


970626-970629



# ARCTIC SEA ICE EXTENT FROM NSCAT/SSM/I

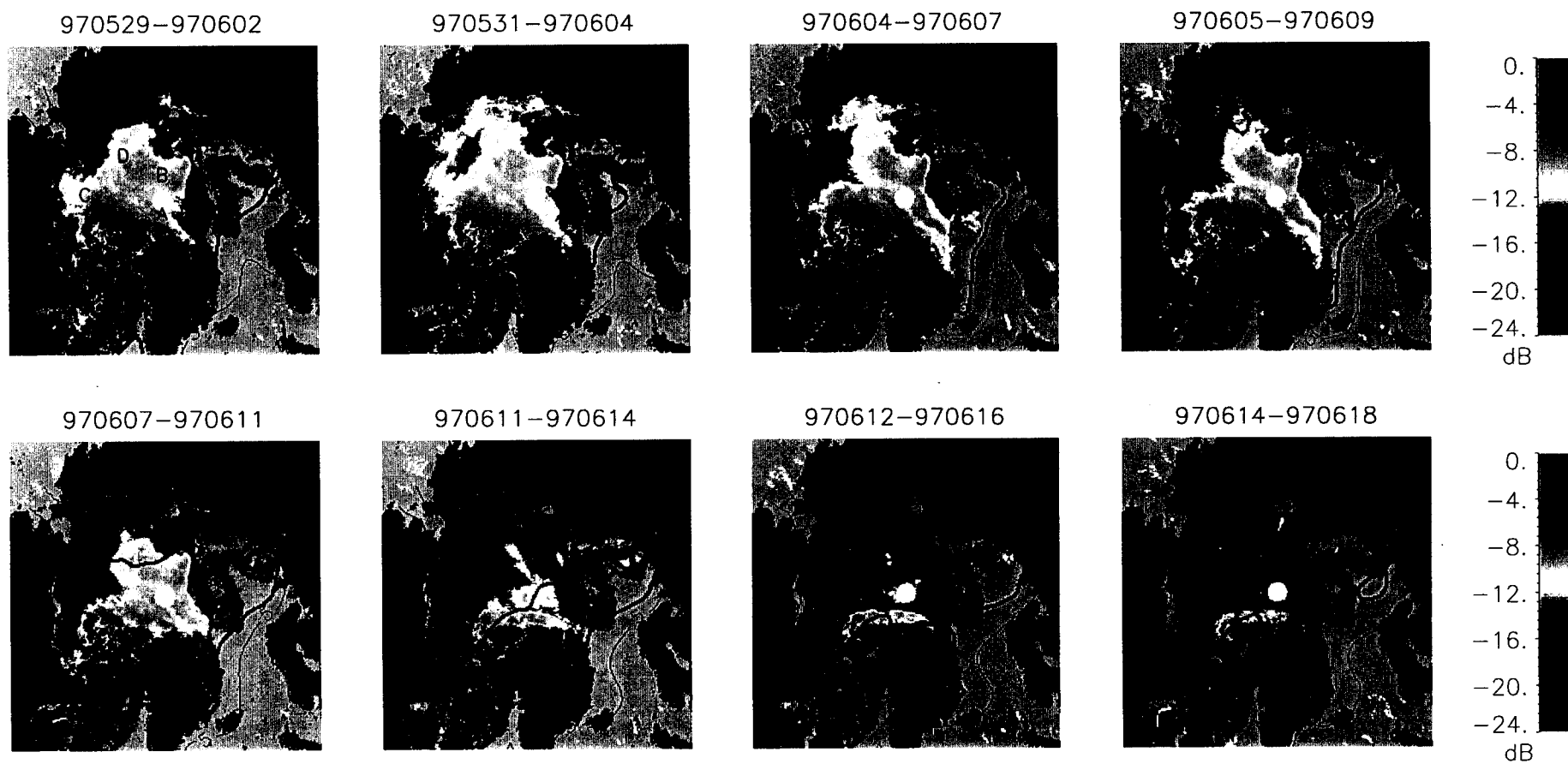
-3000 km < X and Y < 3000 km (SSM/I GRIDS)



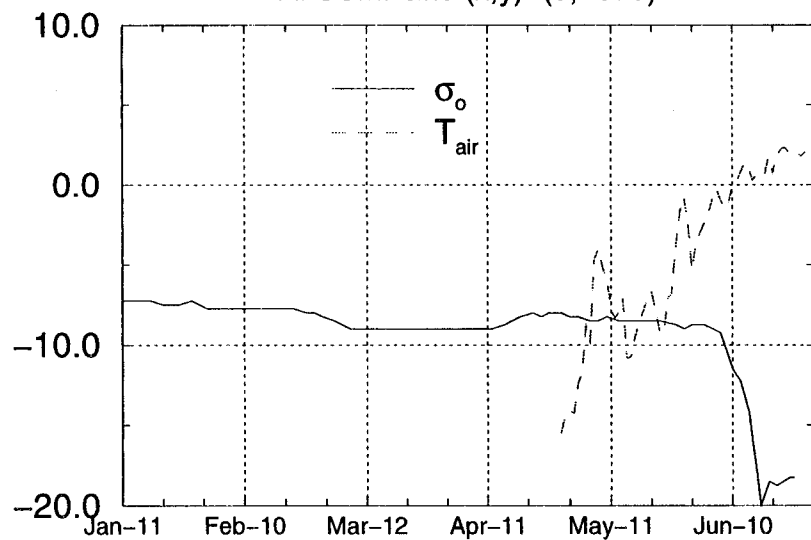
# NSCAT BACKSCATTER DURING MELT ONSET ON ARCTIC SEA ICE

Edge Defined by Polarization and Backscatter

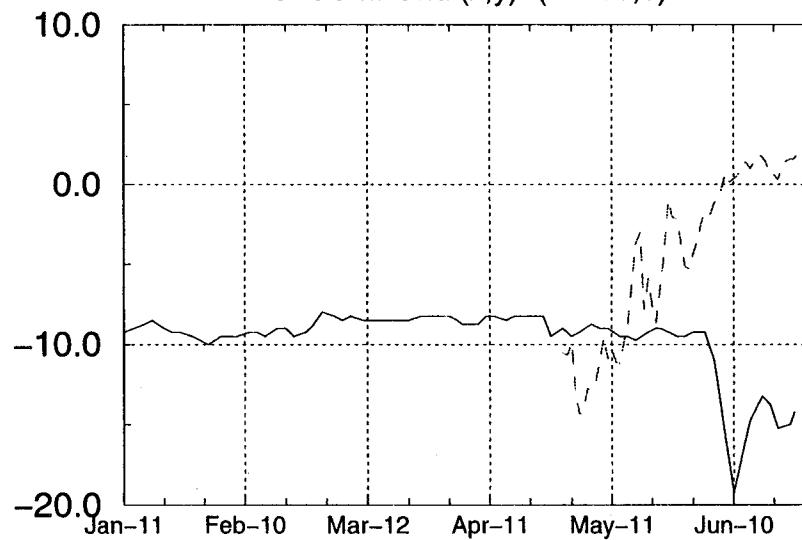
Isotherm From NCEP/NCAR Reanalysis (CDC)



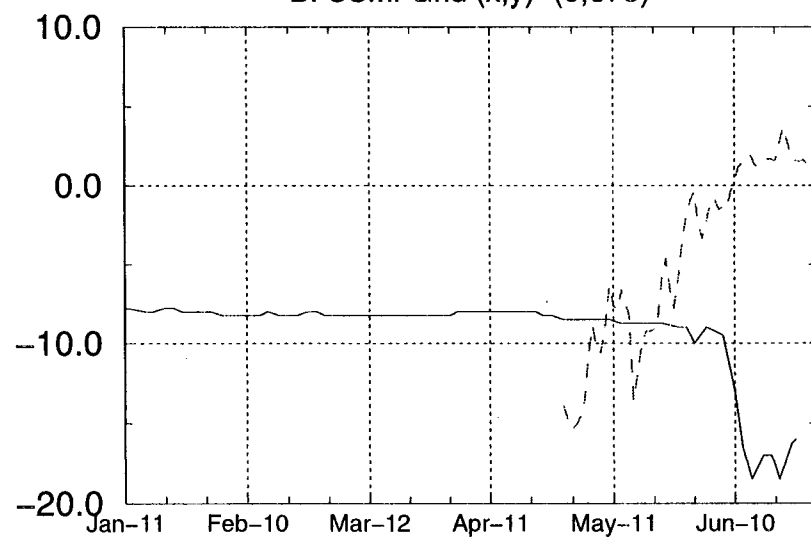
A: SSMI Grid (x,y)=(0,-375)



C: SSMI Grid (x,y)=(-1500,0)



B: SSMI Grid (x,y)=(0,375)



D: SSMI Grid (x,y)=(-750,750)

